A COMPLEX WAVELET-BASED MIMO-OTFS SCHEME FOR JOINT SENSING AND COMMUNICATION LEO SATELLITE

SAIFUR RAHMAN SABUJ[1,2] and HAN-SHIN JO[1]

[1]Department of Automotive Engineering, Hanyang University, Seoul 04763, South Korea
[2]Department of Electrical and Electronic Engineering, Brac University, Dhaka 1212, Bangladesh
E-MAIL: s.r.sabuj@ieee.org and hsjo23@hanyang.ac.kr

Abstract:

This paper investigates a complex wavelet-aided multiple-input and multiple-output orthogonal time-frequency space (CW-MIMO-OTFS) scheme operating in low earth orbit (LEO) satellite systems. We present a mathematical model for the proposed CW-MIMO-OTFS system constructed using a straightforward matrix multiplication approach. The investigation utilized the complex form of the Haar and Daubechies wavelet functions. Additionally, the performance evaluation of the proposed scheme focused on analyzing the bit error rate (BER) and Cramér-Rao bound (CRB) characteristics for joint sensing and communications. The simulation findings demonstrate the superiority of the proposed CW-MIMO-OTFS approach over existing state-of-the-art solutions in terms of the BER and CRB performance compared to the W-MIMO-OTFS scheme in LEO satellite systems.

Keywords:

Bit error rate; complex wavelet; integrated sensing and communication; joint sensing and communication; low earth orbit satellite; orthogonal time frequency space.

1. Introduction

Non-terrestrial networks (NTNs) are critical sixth-generation (6G) cellular networks that complement terrestrial networks and provide global connectivity. 6G cellular networks are likely to integrate non-terrestrial devices such as drones, high-altitude platforms, and low-earth orbit (LEO) satellites [?, ?]. The rapidly evolving channel conditions experienced by LEO satellite (LEO-S) communication systems pose significant challenges because the high relative velocities of these satellites and the dynamic nature of the space environment lead to frequent and significant changes in satellite-to-ground (STG) communication channels [?]. Orthogonal time–frequency space (OTFS) modulation has emerged as a promising solution for addressing the challenges faced by LEO-S communication systems [?]. Moreover, real-world OTFS implementations require substantial computing resources and advanced hardware, particularly complex waveforms or large antenna arrays [?]. The delay-Doppler (DD) channel estimation in OTFS systems can be difficult under rapidly changing channel conditions. A potential solution is to replace the Fourier transform (FT) with a wavelet transform (WT) [?]. This is because WT offers significant advantages over FT in signal analysis. Unlike the FT, which is limited to stationary signals, the WT can be applied to both stationary and nonstationary signals. The efficiency of the WT is attributed to its ability to represent signals with fewer coefficients, resulting in a faster and more effective analysis. This makes WT-based systems more resilient to Doppler shifts, leading to better performance and lower bit-error rates (BER) [?].

Recent research has explored various aspects of OTFS systems for LEO-S communications. OTFS modulation can mitigate Doppler interference in LEO-S communication systems by increasing the number of DD plane bins [?]. Zhang et al. investigated coordinated multi-satellite transmission using OTFS to enhance link performance [?]. Li et al. developed a carrier-frequency offset estimator for OTFS-based LEO-S communication systems to address large-scale Doppler frequency offsets [?]. Arshad et al. presented a solution that leveraged WT-shaped non-orthogonal multiple access (NOMA) within a cell-free massive multiple-input and multiple-output (mMIMO) system to mitigate interference and accommodate a greater number of users [?]. Abid et al. proposed a wavelet-based

OTFS (W-OTFS) system, integrating WT with OTFS modulation using Haar and Daubechies wavelets, which showed enhanced performance in high-mobility wireless channels [?]. The development of a matrix multiplication model for W-OTFS offers several advantages over traditional OTFS, including reduced BER, PAPR, and system complexity. It is compatible with existing OTFS waveforms and features simple modulator/demodulator structures.

In LEO-S networks, OTFS modulation has become a promising method for integrated sensing and communication (ISAC), commonly referred to as joint sensing and communication (JSAC) systems. Li et al. proposed a framework using OTFS for ISAC to determine the target's position and the transmitter's location by taking advantage of DD channel estimation [?]. Zegrar et al. proposed an OTFS-based ISAC scheme for accurate range-velocity profile estimation without requiring large bandwidth or long-duration transmissions [?]. Xia et al. investigated a DD spectrum matching assisted active sensing framework for OTFS-based ISAC systems that achieved better detection and estimation accuracy with fewer computations [?]. Wu et al. proposed a minimum BER precoder design for an OTFS-based ISAC scheme [?].

The benefits of W-OTFS technology have been clarified by the aforementioned work in [?]. However, these were considered in real DWT. Unfortunately, they disregarded the complex wavelet (CW) or complex DWT (CDWT). The creation of a complex input signal requires a CDWT matrix. Compared to real DWT, CDWT offers more precise signal characteristics, enabling superior compression without decomposing the components for complex values [?, ?]. In our initial research, we propose a CDWT-based OTFS (CW-OTFS) scheme to improve the performance of LEO-S systems [?]. In this paper, we propose a CDWT-based MIMO-OTFS (CW-MIMO-OTFS) scheme for improving the performance of LEO-S systems. The main contributions of this study are summarized as follows. (*i*) We propose a new CW-MIMO-OTFS scheme for JSAC system. (*ii*) We present a theoretical analysis of the BER and Cramér-Rao bound (CRB) characteristics of the proposed CW-MIMO-OTFS approach for communication and sensing performance. (*iii*) The simulation results highlight substantial improvements in BER and CRB, which require consideration in CW-MIMO-OTFS-based LEO-S systems.

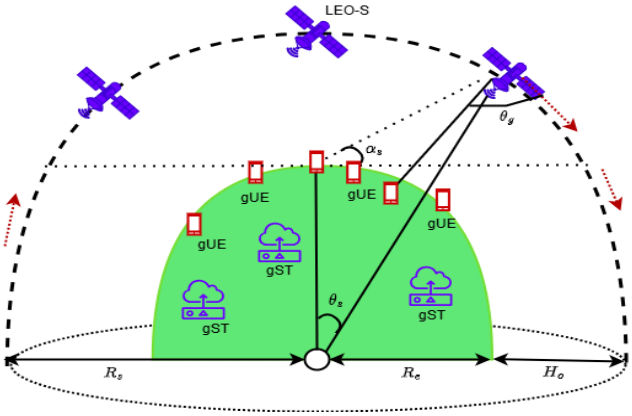

FIGURE 1. The system architecture of CW-MIMO-OTFS scheme for LEO-S scenario.

2. System Model

2.1. Network Architecture

As shown in Fig. 1, we considered an NTN network in which S_l LEO-Ss serve terrestrial G_u gUEs and T_s ground sensing targets (gSTs). In NTN JSAC network, LEO-S can sense and communicate simultaneously. We considered each LEO-S with JSAC capabilities that simultaneously transmits CW-OTFS signals for gUEs and gSTs; and subsequently receives an echo signal from gST, as depicted in Fig. 1. We assume that $\mathcal{S} = \{1, ..., S_l\}$, $\mathcal{G} = \{1, ..., G_u\}$, and $\mathcal{T} = \{1, ..., T_s\}$ are the sets of LEO-Ss, gUEs, and gSTs, respectively. A LEO-S communicates with G_u gUEs using MIMO links. Assuming there is effective isolation between the transmit and receive antennas in LEO-S, the CW-OTFS signals transmitted by the LEO-S do not interfere with those received by the receiving antenna. The gUEs and LEO-Ss were equipped with n_t transmit and n_r receive antennas and distributed within the LEO-S coverage footprint. LEO-Ss are assumed to move clockwise in the same plane with equal radii (R_s) and velocities (v_s). In LEO-S communications, gUE data from data networks are transferred LEO-by-LEO to the serving LEO-S, which then sends it to gUEs via downlink S2G links.

The system utilizes CW-OTFS modulation, where resources are allocated in the DD domain. Each symbol has a frame duration of T and each subcarrier is spaced evenly at intervals of $\Delta f = 1/T$. The resource grid in the DD domain spans T seconds along the delay axis and Δf Hz along the Doppler axis. The grid was divided into M delay

bins and N Doppler bins. Each OTFS frame was assigned to an equivalent OFDM frame in the time-frequency (TF) domain, occupying N OFDM symbols and M subcarriers per symbol [?].

2.2. Channel Model

The distance d_s between a LEO-S and the gUE is derived using the Earth's radius (R_e), LEO-S altitude ($H_o = R_s - R_e$), and the LEO-S's elevation angle (α_s). Using the law of cosines, d_s^g can be derived as [?]

$$d_s^g = \sqrt{R_s^2 + R_e^2 - 2R_s R_e \cos(\theta_s)}, \tag{1}$$

where central angle θ_s ranges between -90^o and 90^o. Regarding the latitude and longitude of the LEO-S and gUE, the θ_s is defined as $\cos(\theta_s) = \cos(L_s)\cos(L_g)\cos(L_{os} - L_{og}) + \sin(L_s)\sin(L_g)$, where L_s and L_{os} denote the latitude and longitude of LEO-S. L_g and L_{og} denote the latitude and longitude of gUE [?]. The free-space path loss L_s incorporates components of the carrier frequency (f_c), d_s^g, and shadow fading (L_{SF}). L_s from the s-th LEO-S to the g-th gUE is computed as [?]

$$L_s^g(dB) = 92.45 + 20\log_{10}(f_c) + 20\log_{10}(d_s^g) + L_{SF}, \tag{2}$$

where f_c is in GHz, and d_s^g is in km. $L_{SF} \sim \mathcal{CN}(0, \sigma_{SF}^2)$, where σ_{SF}^2 represents the variance of shadowing fading.

The channel was modeled as a doubly-selective fading channel with multiple paths (P) defined by the delay and Doppler shifts. The time-varying STG channel for g-th gUE is modeled as [?]

$$\bar{h}_{s,p}^g(\tau, v) = \sum_{p=0}^{P-1} \sqrt{L_s^g} h_{s,p}^g \delta(\tau - \tau_{s,p}^g)\delta(v - v_{s,p}^g), \tag{3}$$

where τ and v represent the delay spread and Doppler shift, respectively. $h_{s,p}^g$ is the complex gain of the p-th path. $l_{s,p}^g$ and $k_{s,p}^g$ represent the delay and Doppler taps of the p-th path from the s-th LEO-S to the g-th gUE, respectively and can be expressed as $l_{s,p}^g = \tau_{s,p}^g M\Delta f$ and $k_{s,p}^g = (v_{s,p}^g f_c/c)\cos(\psi_{s,p}^g)NT$. $\psi_{s,p}^g$ is the the angle between the s-th LEO-S motion direction and the g-th gUE.

The LEO-S channel is modeled in the DD domain, where each path introduces a delay ($\tau_{s,p}^g$) and a Doppler shift ($v_{s,p}^g$). These shifts can be integer or fractional based on their alignment with the DD grid [?]. In the integer delay and Doppler scenario, the delay and Doppler shift for the p-th path are represented as $\tau_{s,p}^g = l_{s,p}^g/M\Delta f$ and $v_{s,p}^g = k_{s,p}^g(c/f_c)/\cos(\psi_{s,p}^g)NT$, respectively. However, the fractional delay and Doppler shift for the p-th path are defined as $\tau_{s,p}^g = (l_{s,p}^g + \alpha_{s,p}^g)/M\Delta f$ and $v_{s,p}^g = (k_{s,p}^g + \beta_{s,p}^g)(c/f_c)/\cos(\psi_{s,p}^g)NT$, respectively. In this case, $\alpha_{s,p}^g$ and $\beta_{s,p}^g$ are commonly assumed to be within the ranges $\alpha_{s,p}^g \in [-0.5, 0.5]$ and $\beta_{s,p}^g \in [-0.5, 0.5]$ [?, ?]. From Eq. (3), the TD channel matrix $\mathbf{H}_{s,p}^g$ can be derived as follows [?]

$$\mathbf{H}_{s,p}^g = \sum_{p=0}^{P-1} \sqrt{L_s^g} h_{s,p}^g \Phi_{l_{s,p}^g + \alpha_{s,p}^g} \Delta_{k_{s,p}^g + \beta_{s,p}^g}, \tag{4}$$

where $\Phi = \text{circ}\left\{[0, 1, \cdots, 0]^{\text{T}}\right\} \in \mathbb{R}^{MN \times MN}$ represents a cyclic shift matrix. $\Delta = \text{diag}[1,\ e^{-2\pi j/MN}, \cdots, e^{-2\pi j(MN-1)/MN}] \in \mathbb{C}^{MN \times MN}$ denotes the diagonal Doppler shift matrix. $\alpha_{s,p}^g = 0$ and $\beta_{s,p}^g = 0$ indicate that there is no fractional delay and Doppler shift.

2.3. CW-MIMO-OTFS Signal

We consider a scenario in which s-th LEO-S transmits a CW-OTFS signal to g-th gUE. We assume that $\mathbf{x}_{dd} \in \mathbb{C}^{MN \times 1}$ be the DD domain of information symbol vector with length MN at s-th LEO-S. The DD domain of information symbol vector can be transformed into symbol matrix $\mathbf{X}_{dd} \in \mathbb{C}^{M \times N}$. The information symbol is created into a TF domain using 2D ICDWT and can be represented as $\mathbf{X}_{tf} = \mathbf{W}_M^c \mathbf{X}_{dd} (\mathbf{W}_N^c)^{\text{H}} \in \mathbb{C}^{M \times N}$, where $\mathbf{W}_M^c$ and $\mathbf{W}_N^c$ are the M-level ICDWT and N-level CDWT matrices. Subsequently, a 1D ICDWT with pulse-shaping waveform $g_{tx}(t)$ is applied to $\mathbf{X}_{tf}$. The TD signal from the s-th LEO-S to the g-th gUE is given by [?]

$$\mathbf{X}_s^g = \mathbf{G}_{tx}(\mathbf{W}_M^c)^{\text{H}} \mathbf{X}_{tf} = \mathbf{G}_{tx} \mathbf{X}_{dd} (\mathbf{W}_N^c)^{\text{H}}, \tag{5}$$

where $\mathbf{G}_{tx} = G_{ta} \cdot \text{diag}\left[g_{tx}(0), \cdots, g_{tx}((M-1)T/M)\right] \in \mathbb{C}^{M \times M}$, where G_{ta} is the LEO-S antenna gain. Following TD conversion, signal matrix, $\mathbf{X}_s^g \in \mathbb{C}^{M \times N}$ is transformed into a signal vector, $\mathbf{x}_s^g \in \mathbb{C}^{n_t MN \times 1}$ for transmission with n_t transmit antenna and can be expressed as

$$\mathbf{x}_s^g = \text{vec}(\mathbf{X}_s^g) = (\mathbf{W}_N^c \otimes \mathbf{G}_{tx})\mathbf{x}_{dd}, \tag{6}$$

where $\otimes$ denotes the Kronecker product. The transmitted signal $\mathbf{x}_s^g$ is sent over a time-varying STG channel. At the receiver, the vectorized transmit-receive signal can be expressed as [?]

$$\mathbf{r}_s^g = \mathbf{H}_{s,p}^g \mathbf{x}_s^g + \mathbf{n}, \tag{7}$$

where $\mathbf{r}_s^g \in \mathbb{C}^{n_r MN \times 1}$ and $\mathbf{H}_{s,p}^g \in \mathbb{C}^{n_r MN \times n_t MN}$. $\mathbf{n} \in \mathbb{C}^{n_r MN \times 1}$ represents the zero mean AWGN noise vector with $\mathcal{CN}(0, N_o \mathbf{I}_{MN})$, where N_o is the noise variance. The noise variance is derived as $N_o = 1/\text{SNR}$, where SNR means signal-to-noise ratio. The received signal vector is transformed into a signal matrix $\mathbf{R} \in \mathbb{C}^{M \times N}$ as $\mathbf{R} = \text{vec}_{M,N}^{-1}(\mathbf{r}_s^g)$. The TF domain signal matrix $\mathbf{Y}_{tf} = \mathbf{W}_M^c \mathbf{G}_{rx} \mathbf{R} \in \mathbb{C}^{M \times N}$ is obtained by applying 1D CDWT. $\mathbf{G}_{rx}$ is the receiver pulse shaping matrix and denoted as $\mathbf{G}_{rx} = G_{ra} \cdot \text{diag}\left[g_{rx}(0), g_{rx}(T/M), \cdots, g_{rx}((M-1)T/M)\right] \in \mathbb{C}^{M \times M}$, where G_{ra} is the gUE antenna gain. From the TF domain signal $\mathbf{Y}_{tf}$, the DD domain signal $\mathbf{Y}$ is obtained by applying the 2D CDWT operation and can be expressed as

$$\mathbf{Y}_s^g = (\mathbf{W}_M^c)^{\text{H}} \mathbf{Y}_{tf} \mathbf{W}_N^c = \mathbf{G}_{rx} \mathbf{R} \mathbf{W}_N^c, \tag{8}$$

From Eq. (6), the DD signal matrix, $\mathbf{Y}_s^g \in \mathbb{C}^{M \times N}$ is transformed into a signal vector, $\mathbf{y}_s^g \in \mathbb{C}^{n_r MN \times 1}$ at n_r receive antenna and can be expressed as

$$\mathbf{y}_s^g = \text{vec}(\mathbf{Y}_s^g) = ((\mathbf{W}_N^c)^{\text{H}} \otimes \mathbf{G}_{rx}) \mathbf{r}_s^g. \tag{9}$$

2.4. Signal Detection

From Eqs. (7) and (5), the vectorized DD received signal at n_r receive antenna can be written as

$$\mathbf{y}_s^g = ((\mathbf{W}_N^c)^{\text{H}} \otimes \mathbf{I}_M)(\mathbf{H}_{s,p}^g \mathbf{x}_s^g + \mathbf{n}) = \mathbf{H}_{DD}^g \mathbf{x}_{dd} + \widetilde{\mathbf{n}}, \tag{10}$$

where $\mathbf{G}_{tx} = \mathbf{G}_{rx} = \mathbf{I}_M$ for rectangular waveforms. $\mathbf{H}_{DD}^g = ((\mathbf{W}_N^c)^{\text{H}} \otimes \mathbf{I}_M) \mathbf{H}_{s,p}^g (\mathbf{W}_N^c \otimes \mathbf{I}_M)$ and $\widetilde{\mathbf{n}} = ((\mathbf{W}_N^c)^{\text{H}} \otimes \mathbf{I}_M)\mathbf{n}$. The receiver has an equalizer for detecting the transmitted information. This study uses an minimum mean square error (MMSE)-based detector, which can be written as [?]

$$\hat{\mathbf{y}}_s^g = \left[(\mathbf{H}_{DD}^g)^{\text{H}} \mathbf{H}_{DD}^g + N_0 \mathbf{I}_{n_t MN}\right]^{-1} (\mathbf{H}_{DD}^g)^{\text{H}} \mathbf{y}_s^g. \tag{11}$$

Finally, the maximum-likelihood (ML) detection estimates the information symbol vector x_{dd} as one that minimizes the distance between $\hat{\mathbf{y}}_s^g$ and x_{dd}, which can be mathematically expressed as follows:

$$\hat{\text{x}}_{dd} = \underset{\text{x}_{dd} \in \Psi^{MN}}{\arg\min} \left\| \hat{\mathbf{y}}_s^g - \text{x}_{dd} \right\|^2, \tag{12}$$

where Ψ^{MN} is the set of all possible transmitted vectors (constellation points) of length MN.

2.5. BER Analysis

According to [?, ?], the input-output relation using Eqs. (4) and (10) for analyzing the diversity of the proposed CW-MIMO-OTFS can be stated as

$$\mathbf{y}_s^g = \mathbf{H}_{DD}^g \mathbf{x}_{dd} + \widetilde{\mathbf{n}} = \mathbf{\Omega}(\mathbf{x}_{dd}) \mathbf{h}_s^g + \widetilde{\mathbf{n}}, \tag{13}$$

where $\mathbf{\Omega}(\mathbf{x}_{dd}) = [\mathbf{\Omega}_0(\mathbf{x}_{dd}^1), \cdots, \mathbf{\Omega}_0(\mathbf{x}_{dd}^{n_t})] \in \mathbb{C}^{n_r MN \times n_r n_t P}$, $\mathbf{\Omega}_0(\mathbf{x}_{dd}^t) = [\mathbf{\Gamma}_1 \mathbf{x}_{dd}^t \mid \cdots \mid \mathbf{\Gamma}_P \mathbf{x}_{dd}^t] \in \mathbb{C}^{MN \times P}$, $\mathbf{\Gamma}_p = ((\mathbf{W}_N^c)^{\text{H}} \otimes \mathbf{I}_M) \Phi_{l_{s,p}^g + \alpha_{s,p}^g} \Delta_{k_{s,p}^g + \beta_{s,p}^g} (\mathbf{W}_N^c \otimes \mathbf{I}_M) \in \mathbb{C}^{MN \times MN}$, $\mathbf{h}_s^g = [(\mathbf{h}_{11}^g)^{\text{T}}, (\mathbf{h}_{n_r 1}^g)^{\text{T}}, \cdots, (\mathbf{h}_{n_r n_t}^g)^{\text{T}}]^{\text{T}} \in \mathbb{C}^{n_r n_t P \times 1}$, and $\mathbf{h}_{so}^g = [h_{s,1}^g, h_{s,2}^g, \cdots, h_{s,P}^g] \in \mathbb{C}^{P \times 1}$.

Given perfect channel state information (CSI) at g-th gUE, the conditional pairwise error probability (PEP) for the above system - that is, the likelihood of sending x_{dd} but selecting $\hat{\text{x}}_{dd}$ incorrectly - is determined by [?]

$$\Pr(\text{x}_{dd} \to \hat{\text{x}}_{dd} | \mathbf{h}_s^g) = \mathbb{Q}\left(\sqrt{\frac{\left\| [\mathbf{\Omega}(\mathbf{x}_{dd}) - \mathbf{\Omega}(\hat{\mathbf{x}}_{dd})] \mathbf{h}_s^g \right\|^2}{2N_o}} \right), \tag{14}$$

where $\mathbb{Q}(\cdot)$ is the Q-function or Gaussian tail function and $N_o = 1/\text{SNR}$. This is the probability that, given x_{dd} transmitted on a channel with parameters $\mathbf{h}_s^g$, the Euclidean distance of the received signal $\mathbf{y}_s^g$ from $\mathbf{\Omega}(\hat{\mathbf{x}}_{dd})$ is less than its distance from $\mathbf{\Omega}(\mathbf{x}_{dd})$ [?].

Using the Chernoff upper bound [?], the conditional PEP can be reduced as

$$\Pr(\text{x}_{dd} \to \hat{\text{x}}_{dd}) \leq \mathbb{E}_{\mathbf{h}_s^g}\left[\exp\left(-\frac{\left\| \mathbf{\Omega}(\boldsymbol{\delta}) \mathbf{h}_s^g \right\|^2}{4N_o} \right) \right], \tag{15}$$

where $\mathbf{\Omega}(\boldsymbol{\delta}) = \mathbf{\Omega}(\mathbf{x}_{dd}) - \mathbf{\Omega}(\hat{\mathbf{x}}_{dd})$ and $\boldsymbol{\delta} = \mathbf{x}_{dd} - \hat{\mathbf{x}}_{dd}$. $\Pr(\cdot)$ denotes the probability function. The expectation implies $\mathbb{E}_{\mathbf{h}_s^g}[\cdot]$ that this becomes an unconditional PEP when averaged over all channel realizations.

Based on [?], the average BER is approximated by adding all possible PEPs weighted by their bit error distances [?]. The average BER P_b for the CW-MIMO-OTFS system is calculated using the unconditional PEP [?] and can be stated as

$$P_b \leq \frac{1}{\mathcal{Q}^{MN}} \sum_{\text{x}_{dd} \in \Psi^{MN}} \sum_{\text{x}_{dd} \neq \hat{\text{x}}_{dd}} \frac{d_e(\text{x}_{dd}, \hat{\text{x}}_{dd})}{N_b} \cdot \left(\prod_{j=1}^{R(\text{x}_{dd}, \hat{\text{x}}_{dd})} \lambda_j \right)^{-n_r} \left(\frac{1}{4N_o P} \right)^{-n_r R(\text{x}_{dd}, \hat{\text{x}}_{dd})}, \tag{16}$$

where Ψ represents $\mathcal{Q}$-ary signal constellation wherein x_{dd} becomes $\mathrm{x}_{dd} \in \Psi^{MN}$. $N_b = MN\log_2(\mathcal{Q})$ denotes the total number of bits transmitted in one CW-OTFS frame. $d_e(\mathrm{x}_{dd}, \hat{\mathrm{x}}_{dd})$ is the difference in number of information bits between x_{dd} and $\hat{\mathrm{x}}_{dd}$).

2.6. CRB Analysis

At the same time, the CW-OTFS waveform is also radiated and reflected by the gST for tracking purposes. According to [?], the reflected echo signal at the LEO-S from t-th gST can be expressed as

$$\mathbf{y}^t_{s,e} = \mathbf{H}^t_{DD,e}\mathbf{x}_{dd} + \widetilde{\mathbf{n}}_e, \tag{17}$$

where $\mathbf{H}^t_{DD,e}$ is the corresponding DD domain LEO-S channel between the LEO-S and the gST and is defined as $\mathbf{H}^t_{DD} = ((\mathbf{W}^c_N)^{\mathrm{H}} \otimes \mathbf{I}_M)\mathbf{H}^t_{s,p}(\mathbf{W}^c_N \otimes \mathbf{I}_M)$ and $\mathbf{H}^t_{s,p} = \sum_{p=0}^{P-1}\sqrt{L^t_s}h^t_{s,p}\Phi_{l^t_{s,p}+\alpha^t_{s,p}}\Delta_{k^t_{s,p}+\beta^t_{s,p}}$, $\forall t$. It also travels double distance due to reflection from the gST. $\widetilde{\mathbf{n}}_e$ represents the zero mean AWGN noise vector with $\mathcal{CN}(0, N_{o,e}\mathbf{I}_{MN})$, where $N_{o,e}$ is the noise variance.

According to CRB theory [?], complex Gaussian vectors have a mean $\boldsymbol{\mu}$ that depends on parameter $\nu^t_{s,p}$ and a covariance $\mathbf{R}_{MN}$ that is independent of $\nu^t_{s,p}$. From the CRB theory, the Fisher information can be expressed as $\mathcal{I}(\nu^t_{s,p}) = \frac{1}{2}\mathrm{tr}\left(\mathbf{R}^{-1}_{MN}\frac{\partial\mathbf{R}_{MN}}{\partial\nu^t_{s,p}}\mathbf{R}^{-1}_{MN}\frac{\partial\mathbf{R}_{MN}}{\partial\nu^t_{s,p}}\right)\Re\left\{\frac{\partial\boldsymbol{\mu}^{\mathrm{H}}}{\partial\nu^t_{s,p}}\mathbf{R}^{-1}_{MN}\frac{\partial\boldsymbol{\mu}}{\partial\nu^t_{s,p}}\right\}$. Since $\mathbf{R}_{MN} = N_{o,e}\mathbf{I}_{MN}$ is independent of $\nu^t_{s,p}$, the first term is zero, and we have

$$\mathcal{I}(\nu^t_{s,p}) = \Re\left\{\frac{\partial\boldsymbol{\mu}^{\mathrm{H}}}{\partial\nu^t_{s,p}}\mathbf{R}^{-1}_{MN}\frac{\partial\boldsymbol{\mu}}{\partial\nu^t_{s,p}}\right\}. \tag{18}$$

Consider $\boldsymbol{\mu} = \mathbf{H}^t_{DD,e}\mathbf{x}_{dd}$. Thus, $\frac{\partial\boldsymbol{\mu}}{\partial\nu^t_{s,p}} = \frac{\partial\mathbf{H}^t_{DD,e}}{\partial\nu^t_{s,p}}\mathbf{x}_{dd} = \dot{\mathbf{H}}^t_{DD,e}\mathbf{x}_{dd}$. Similarly, $\frac{\partial\boldsymbol{\mu}^{\mathrm{H}}}{\partial\nu^t_{s,p}} = (\dot{\mathbf{H}}^t_{DD,e})^{\mathrm{H}}\mathbf{x}^{\mathrm{H}}_{dd}$. Putting the value of $\frac{\partial\boldsymbol{\mu}^{\mathrm{H}}}{\partial\nu^t_{s,p}}$, $\mathbf{R}_{MN}$, and $\frac{\partial\boldsymbol{\mu}}{\partial\nu^t_{s,p}}$ in (18), the $\mathcal{I}(\nu^t_{s,p})$ can be written as

$$\mathcal{I}(\nu^t_{s,p}) = \frac{1}{N_{o,e}}\Re\left\{\mathbf{x}^{\mathrm{H}}_{dd}(\dot{\mathbf{H}}^t_{DD,e})^{\mathrm{H}}\mathbf{H}^t_{DD,e}\mathbf{x}_{dd}\right\}, \tag{19}$$

where $\dot{\mathbf{H}}^t_{DD,e} = \sum_{p=0}^{P-1}\sqrt{L^t_s}h^t_{s,p}((\mathbf{W}^c_N)^{\mathrm{H}} \otimes \mathbf{I}_M)\mathbf{D}_\nu\Phi_{l^t_{s,p}+\alpha^t_{s,p}}\ \Delta_{k^t_{s,p}+\beta^t_{s,p}}(\mathbf{W}^c_N \otimes \mathbf{I}_M)$, $\forall t$. $\mathbf{D}_\nu$ is the diagonal matrix of Doppler derivative and can be defined as $\mathbf{D}_\nu = \mathrm{diag}\left(j\frac{2\pi T f_c\cos(\psi^t_{s,p})}{cM}[0, 1, \cdots, MN-1]\right)$. The CRB is the inverse of $\mathcal{I}(\nu^t_{s,p})$ and can be written from Eq. (19) as follows

$$\mathrm{CRB} = \frac{1}{\mathcal{I}(\nu^t_{s,p})} = \left(\frac{1}{N_{o,e}}\Re\left\{\mathbf{x}^{\mathrm{H}}_{dd}(\dot{\mathbf{H}}^t_{DD,e})^{\mathrm{H}}\mathbf{H}^t_{DD,e}\mathbf{x}_{dd}\right\}\right)^{-1}. \tag{20}$$

3. Performance Evaluation

We considered a scenario with 10 LEO-Ss in a single orbit implemented in MATLAB. The 10 LEO-Ss were deployed in the same orbital plane with regular spacing, forming a total deployment angle of 36 degrees. The orbital altitude was set to 700 km, and the speed of each LEO-S was set to $v_s = 7.4$ km/s. For this simulation, 50 gUEs and 5 gSTs were randomly distributed within the South Korean region. The LEO-S coordinate is taken into account $(35.28°, 126.53°)$. To compare our findings, we take into account three CWs, including Haar, Daubechies D4, and Daubechies D8. A detailed explanation of the simulation scenario is found in [?].

The frame size for the CW-MIMO-OTFS transmission was set to $M = 8$ and $N = 8$. The central frequency was configured at 2 GHz (S band), with a subcarrier spacing of 60 kHz. The LEO-S and gUE antenna gains were 40 and 35 dBi, respectively. All LEO-S links were modeled using the 3GPP NTN TDLA100 model [?], and included three pathways with Rayleigh fading. For Rayleigh fading, it was assumed that the fading variance was 3 dB in (2), and the path loss for each channel was calculated using Eqs. (1) and (2). In addition, the channel gain for each link was generated using Eqs. (1), (2), and (4). In this simulation, we used integer delay and Doppler taps, thus $\alpha^g_{s,p} = \alpha^t_{s,p} = 0$ and $\beta^g_{s,p} = \beta^t_{s,p} = 0$.

3.1. Performance of the Proposed CW-OTFS

Figure 2 presents the average BER performance versus SNR for different numbers of spectral efficiencies (SE) and various CWs for perfect CSI. The SE was set to 1, 2, or 3 b/s/Hz. From the simulation results, it was observed that the average BER rapidly decreased with increasing SNR for all SEs. For all CWs, an SE of 1 b/s/Hz showed better performance than SEs of 2 b/s/Hz and 3 b/s/Hz. This suggests that a lower SE (low-order modulation) improves performance with increasing SNR. Furthermore, CW-MIMO-OTFS with Haar consistently achieved a lower BER than D4 and D8. Moreover, the CW-MIMO-OTFS with Haar exhibited a lower BER for all SEs. By

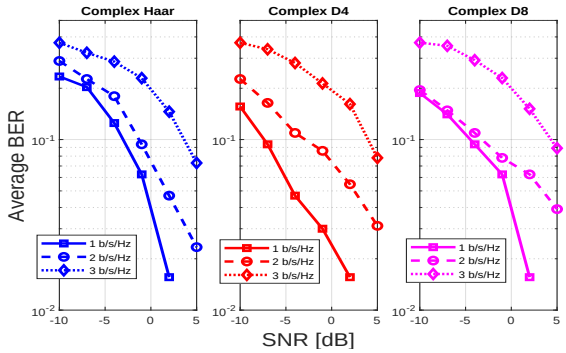

FIGURE 2. Average BER performance under various CW and SE for perfect CSI.

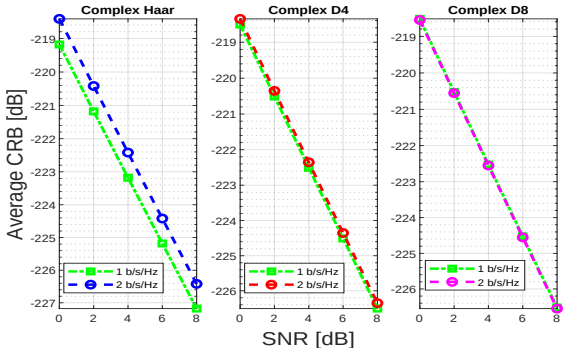

FIGURE 3. Average CRB performance under various CW and SE for perfect CSI.

comparison, it was demonstrated that CW-MIMO-OTFS with the Haar system maintained good performance across all SEs.

Figure 3 presents the average CRB performance versus SNR for different numbers of SE and various CWs for perfect CSI. The SE was set to 1 and 2 b/s/Hz. From the simulation results, it was observed that the average CRB rapidly decreased with increasing SNR for all SEs, indicating that the sensing quality-of-service can be satisfied. A lower CRB indicates that the highest feasible accuracy for determining parameters such as delay or Doppler increases as noise power decreases. For all CWs, an SE of 1 b/s/Hz showed better performance than SEs of 2 b/s/Hz. This suggests that a lower SE (low-order modulation) improves performance with increasing SNR. Furthermore, CW-MIMO-OTFS with Haar consistently achieved a lower CRB than D4 and D8. By comparison, it was demonstrated that CW-MIMO-OTFS with the Haar system maintained good performance across all SEs.

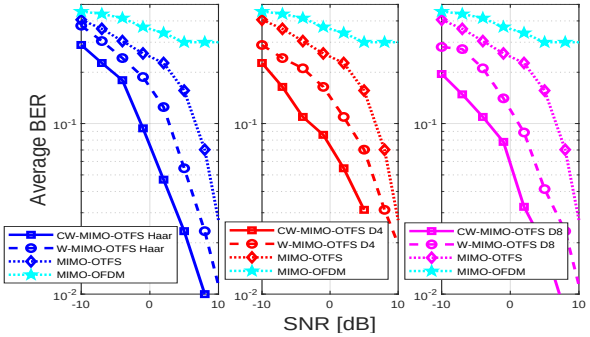

FIGURE 4. Average BER comparison of various schemes for perfect CSI scenario.

3.2. Comparison with Other Schemes

Figure 4 presents a comparison of the average BER among CW-MIMO-OTFS, W-MIMO-OTFS, MIMO-OTFS, and MIMO-OFDM for a perfect CSI. In this scenario, an SE of 2 b/s/Hz and a frame size of $(M, N) = (8, 8)$ were considered. It was observed that CW-MIMO-OTFS exhibited significant BER reductions compared to W-MIMO-OTFS, MIMO-OTFS, and MIMO-OFDM at 2 b/s/Hz. For example, CW-MIMO-OTFS with Haar offered 133.76%, 576.52%, and 1182.05% BER reductions compared to W-MIMO-OTFS with Haar, MIMO-OTFS, and MIMO-OFDM, respectively, at an SNR of 5 dB. In addition, CW-MIMO-OTFS with D8 offered 116.23%, 717.80%, and 1470.68% BER reductions compared to W-MIMO-OTFS with D8, MIMO-OTFS, and MIMO-OFDM, respectively, at an SNR of 5 dB. This observation confirmed that CW-MIMO-OTFS showed significant BER reductions compared with the other schemes.

Figure 5 presents a comparison of the average CRB among CW-MIMO-OTFS, W-MIMO-OTFS, MIMO-OTFS, and MIMO-OFDM for a perfect CSI. It was observed that CW-MIMO-OTFS exhibited significant CRB reductions compared to W-MIMO-OTFS, MIMO-OTFS, and OFDM at 2 b/s/Hz and $(M, N) = (8, 8)$. For example, CW-MIMO-OTFS with Haar offered 3.39%, 5.90%, and 9.66% CRB reductions compared to W-MIMO-OTFS with Haar, MIMO-OTFS, and MIMO-OFDM, respectively, at an SNR of 10 dB. In addition, CW-MIMO-OTFS with D8 offered 3.38%, 5.96%, and 9.71% CRB reductions compared to W-MIMO-OTFS with D8, MIMO-OTFS, and MIMO-OFDM, respectively, at an SNR of 10 dB. This observation confirmed that CW-MIMO-OTFS showed significant CRB reductions compared with the other schemes.

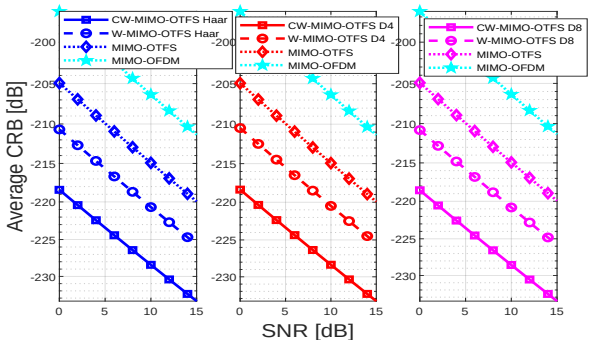

FIGURE 5. Average CRB comparison of various schemes for perfect CSI scenario.

4. Conclusion

This paper presented a CW-MIMO-OTFS approach for the LEO-S system. The integration of CDWT into the MIMO-OTFS framework yielded consistent improvements in both the BER and CRB. In addition, the CW-MIMO-OTFS design replaced the FT-based ISFFT of the traditional OTFS, thereby reducing the computational complexity. Moreover, the use of CWs provides an adaptable tradeoff between time and frequency resolutions for higher-order modulation techniques, allowing the proposed approach to effectively mitigate both the delay and Doppler spread in the LEO-S system. The simulation results demonstrated that the proposed CW-MIMO-OTFS system achieved significant BER improvements compared with the W-MIMO-OTFS, MIMO-OTFS, and MIMO-OFDM approaches. The CW-MIMO-OTFS scheme with Haar wavelets exhibited BER reductions of 133.76%, 576.52%, and 1182.05% relative to the W-MIMO-OTFS with Haar, MIMO-OTFS, and MIMO-OFDM systems, respectively, at an SNR of 5 dB.

Acknowledgements

This research was supported in part by Brain Pool Program funded by the Ministry of Science and ICT through the National Research Foundation of Korea (RS-2024-00447104) and in part by Korea Research Institute for Defense Technology Planning and Advancement (KRIT) grant funded by the Korea government (DAPA (Defense Acquisition Program Administration)) (KRIT-CT-22-047, Space-Layer Intelligent Communication Network Laboratory, 2022)